Transcriptomic profiling of sex-specific olfactory neurons reveals subset-specific receptor expression in *C. elegans*

Author Names and Affiliations:

Douglas K. Reilly[1,7,†], Erich M. Schwarz[2,†], Caroline S. Muirhead[1], Annalise N. Robidoux[1,3], Igor Antoshechkin[4], Anusha Narayan[4,5], Meenakshi K. Doma[4,6], Paul W. Sternberg[4], Jagan Srinivasan[1,8,*]

[1] Department of Biology and Biotechnology, Worcester Polytechnic Institute, Worcester, MA 01605, USA

[2] Department of Molecular Biology and Genetics, Cornell University, Ithaca, NY 14853, USA

[3] Department of Chemistry and Biochemistry, Worcester Polytechnic Institute, Worcester, MA 01605, USA

[4] Division of Biology and Biological Engineering, California Institute of Technology, Pasadena, CA 91125

[5] Present address: Strategic Marketing, Evidation Health, San Mateo, CA 94402, USA

[6] Present address: Genomics Lead, Individualized Cell and Gene Therapies, South San Francisco, Genentech, CA 94080, USA

[7] Present address: Biology Department, Tufts University, Medford, MA 02155, USA

[8] Program of Bioinformatics and Computational Biology, Worcester Polytechnic Institute, Worcester, MA 01605, USA

* Corresponding author

[†] These authors contributed equally to this work

Short Title: Male pheromone G protein-coupled receptors in *C. elegans*

Key words: *C. elegans*, Pheromone, Sex-specific, G Protein-Coupled Receptors, Transcriptomes, Single-Cell

Corresponding author:

Jagan Srinivasan

Life Sciences and Bioengineering Center, 4th Floor

60 Prescott Street, Worcester, MA, 01605

(508) 831-6564

jsrinivasan@wpi.edu

SUMMARY

The nematode *Caenorhabditis elegans* utilizes chemosensation to navigate an ever-changing environment for its survival. A class of secreted small-molecule pheromones, termed ascarosides, play an important role in olfactory perception by affecting a host of biological function ranging from development to behavior. The ascaroside ascr#8 mediates sex-specific behaviors, driving avoidance in hermaphrodites and attraction in males. Males sense ascr#8 via the ciliated male-specific cephalic sensory (CEM) neurons, which exhibit radial symmetry along dorsal-ventral and left-right axes. Calcium imaging studies suggest a complex neural coding mechanism that translates stochastic physiological responses in these neurons to reliable behavioral outputs. To test the hypothesis that the neurophysiological complexity arises from differential expression of genes within subsets of these neurons, we performed cell-specific transcriptomic profiling of these sensory neurons. Expression profiling revealed between 20 and 639 genes enriched at least two-fold per CEM neuron and identified multiple G protein coupled receptor (GPCR) candidates enriched in non-overlapping subsets of CEM neurons. GFP reporter analysis confirmed that RNA expression of two of the GPCR genes, *srw-97* and *dmsr-12*, is enriched in specific subsets of the CEM neurons. Single CRISPR-Cas9 knockouts of either *srw-97* or *dmsr-12* resulted in partial defects, while a double knockout of both *srw-97* and *dmsr-12* completely abolished the attractive response to ascr#8, suggesting that each receptor acts in a non-redundant manner in discrete olfactory neurons. Together, our results suggest that the evolutionarily distinct GPCRs SRW-97 and DMSR-12 act to facilitate male-specific sensation of ascr#8 through discrete subsets of CEM neurons.

INTRODUCTION

The ability of an organism to find a mate is critical to the survival of a species. Many species utilize small molecule pheromones to signal mate location (PUNGALIYA *et al.* 2009; NARAYAN *et al.* 2016), sexual maturity (APRISON AND RUVINSKY 2015; APRISON AND RUVINSKY 2017), and receptivity (HOUCK *et al.* 2007; JANG *et al.* 2017). These signals are sensed and processed through the nervous system to generate proper behavioral and developmental responses. The nematode *Caenorhabditis elegans* communicates with conspecifics almost exclusively using pheromones called ascarosides (LUDEWIG *et al.* 2019; MCGRATH AND RUVINSKY 2019).

Ascarosides are a large, structurally conserved class of small molecule pheromones (VON REUSS AND SCHROEDER 2015; ZHANG *et al.* 2017). Built in a modular fashion, they are composed of a core ascarylose sugar and a fatty-acid derived side chain (BUTCHER *et al.* 2007; VON REUSS *et al.* 2012; LUDEWIG *et al.* 2019). Ascarosides signal a host of environmental and developmental information, including the sexual maturity and location of potential mates (NARAYAN *et al.* 2016; APRISON AND RUVINSKY 2017). This communication system is conserved across nematodes, with different species using different combinations of ascarosides or structural derivatives (CHOE *et al.* 2012; RAGSDALE *et al.* 2013; DONG *et al.* 2016; DONG *et al.* 2018; REILLY *et al.* 2019). While the effects of some ascarosides are dependent on physiological state (BUTCHER *et al.* 2009; BUTCHER 2017; CHUTE *et al.* 2019), others are able to elicit sex-specific responses (PUNGALIYA *et al.* 2009; NARAYAN *et al.* 2016; FAGAN *et al.* 2018).

Most neurons in the *C. elegans* nervous system are bilaterally symmetrical (WHITE *et al.* 1986), though radially symmetric classes of sensory neurons exist, such as the inner labial (IL1 and IL2) neurons (HRUS *et al.* 2007; WANG *et al.* 2014; WANG *et al.* 2015) which are required for normal dauer development, nictation behavior, and foraging (LEE *et al.* 2012; SCHROEDER *et al.*

2013). *C. elegans* also has several sex-specific neurons, such as the HSN neuron (hermaphrodite-specific neuron) involved in egg laying (APIRSON AND RUVINSKY 2019a; APIRSON AND RUVINSKY 2019b), and the MCM neurons in the male that contribute to neuronal plasticity and learning (SAMMUT *et al.* 2015). However, while most male-specific neurons are located in the tail, the major contributor to male-specific behaviors are the chemosensory CEM neurons, located in the amphid.

These four radially symmetric neurons have been found, through laser ablation, electrophysiology, and calcium imaging studies to be involved in sensing the ascaroside pheromones ascr#8 and ascr#3 (PUNGALIYA *et al.* 2009; NARAYAN *et al.* 2016; REILLY *et al.* 2017). Ascr#3 plays a role in dauer formation, functioning alongside ascr#2 and ascr#4 as the "dauer pheromone" (BUTCHER *et al.* 2008). Ascr#8, meanwhile, is unique in that it contains a *p*-aminobenzoic acid moiety on its terminus (PUNGALIYA *et al.* 2009; ARTYUKHIN *et al.* 2018). We have previously shown by both laser and genetic ablation experiments that ascr#8 is sensed primarily by male-specific CEM neurons located in the head region of the male nervous system (NARAYAN *et al.* 2016). In animals lacking CEM (through either genetic or laser ablation), the response to ascr#8 is abolished, and further ablation of the ASK results in complete loss of the ascr#3 response (NARAYAN *et al.* 2016). Through studies ablating three of the four CEM neurons, leaving one CEM neuron intact, it was found that four CEM neurons cooperate to drive a tuned response to an intermediate, 1 μM concentration of both ascr#3 and ascr#8 (NARAYAN *et al.* 2016).

Although CEM neurons are indeed the primary pathway by which male *C. elegans* sense and response to ascr#8, this response is modulated by additional neural circuitry via neuropeptides. The FMRFamide-like peptide gene *flp-3* encodes ten discrete peptides, some of which act through two neuropeptide receptors both to repress *C. elegans*' normal avoidance of ascr#8, and to

simultaneously make *C. elegans* positively attracted to ascr#8 (REILLY *et al.* 2021). However, it remains unknown how CEM neurons themselves sense and drive responses to ascr#8.

Calcium imaging and electrophysiological experiments demonstrated that CEM neurons show variable responses to stimuli not only between different animals, but within a single animal (NARAYAN *et al.* 2016; REILLY *et al.* 2017). While other neurons such as the stochastically asymmetric AWC chemosensory neurons show variable calcium responses between different animals, these responses are consistent between the left and right AWC neurons of a single animal (COCHELLA *et al.* 2014). In contrast, we have observed that responses of individual CEM neurons are stochastic within single animals, and yet four CEM neurons within one animal are somehow consistently able to generate proper behavioral responses to both ascr#3 and ascr#8 (NARAYAN *et al.* 2016). To understand this remarkable pattern of stochastic neuronal activity yielding consistent neuronal outputs, it is imperative to uncover genes encoding components of the CEM response.

A recent study in *C. elegans* hermaphrodites generated transcriptomic landscapes of 118 neuronal classes from 302 neurons in order to link functional and anatomical properties of individual neurons with their molecular identities (TAYLOR *et al.* 2021). Discrete neuronal classes were successfully identified via their combinations of expressed neuropeptides and neuropeptide receptor genes. However, a similar feat is yet to be performed on male *C. elegans*, and the transcriptomic profiles of male neurons remain enigmatic.

In a more focused transcriptomic approach, gene expression profiles of extracellular vesicle-releasing neurons (EVNs) as a whole were determined by expressing GFP under the EVN-specific *klp-6* promoter, mechanically and proteolytically dissociating male worms expressing this GFP, selecting the target GFP^+ neurons with FACS, and performing RNA-seq on the collected GFP^+ neurons (WANG *et al.* 2015; KALETSKY *et al.* 2016). This gave thousands of EVNs in each

biological replicate and offered increased statistical power in analyzing transcriptional landscapes. CEM neurons are a subset of EVN neurons, so CEM transcriptomic data are embedded in these data, but the expression values of CEM and EVN are not equivalent.

To begin understanding how CEM neurons achieve stochastic yet reliable physiological responses to ascr#8, we performed single-cell RNA-seq (SCHWARZ *et al.* 2012) on male-specific CEM neurons. We uncovered a small number of genes encoding G protein-coupled receptors (GPCRs) highly enriched in single CEM neurons. Given that all ascaroside receptors identified to date have been GPCRs (KIM *et al.* 2009; MCGRATH *et al.* 2011; PARK *et al.* 2012; GREENE *et al.* 2016a; GREENE *et al.* 2016b; CHUTE *et al.* 2019), we tested whether any of these enriched genes contribute to male *C. elegans* sensation of ascr#8. Through neuronal RNAi knockdown and CRISPR null mutagenesis, we identified two distantly related GPCR genes that contribute to the ascr#8 behavioral response, *srw-97* and *dmsr-12*; expression of these genes are enriched in ventral and dorsal CEMs, respectively. When expression of each receptor was knocked down through RNAi, behavioral responses to ascr#8 were partially deficient. Using CRISPR and genetic crosses to generate a double *srw-97 dmsr-12* mutant, we found that loss of both receptors results in a complete loss of behavioral response to ascr#8. Phylogenetic analysis further indicates that both receptors are homologous to closely related receptors across the *Caenorhabditis* genus, and robust ascr#8 responses may be a trait recently evolved in *C. elegans*.

RESULTS

The transcriptomic landscape of CEM neurons is variable

Individual CEM neurons were isolated from *C. elegans* expressing an integrated GFP labeling extracellular vesicle-releasing neurons (EVNs, p*pkd-2*::GFP [**Figure 2A**]), as previously

described (GOODMAN *et al.* 1998; NARAYAN *et al.* 2011; NARAYAN *et al.* 2016). Cells were separated by anatomical identity (i.e., CEM dorsal left [DL], dorsal right [DR], ventral left [VL], and ventral right [VR]), and cDNA libraries were constructed.

Enriched genes in each CEM neuron were identified by comparing RNA-seq profiles of distinct CEM types; genes expressed at least two times more strongly in one CEM type than others were listed and checked for biological functions, as annotated by their WormBase Gene Ontology (GO) terms (HARRIS *et al.* 2020; GENE ONTOLOGY 2021). A variety of enriched gene sets were defined for different CEM neurons, ranging from 20 genes enriched in CEM VL to over 600 in CEM VR (**Table S1, S6, S7**). Dorsal CEM neurons were more consistent, expressing 98 and 105 enriched genes in the right and left neurons, respectively (**Table S1, S8, S9**). Uniquely mapped reads ranged from 1.9 to 3.8 million per CEM type, matching the trend for alignment rates of each CEM neuron, which ranged from 19.73% to 48.01%, (**Table S2**) with an average of 1.410 genes showing robust RNA expression in each neuron (**Table S3**).

Five genes encoding G protein-coupled receptors (*seb-3, srr-7, srw-97, dmsr-12, srd-32*) were expressed at levels four times higher in one CEM neuron than in other CEM neurons. Of these, four were uncharacterized; one (*seb-3*) has previously been shown to play roles in locomotion, stress response, and ethanol tolerance (JEE *et al.* 2013). *dmsr-12* is related to *daf-37* (ROBERTSON AND THOMAS 2006), a previously identified ascaroside receptor gene (PARK *et al.* 2012), although it is more closely related to the neuropeptide receptor gene *dmsr-1*, and more distantly to *srw-97* (ROBERTSON AND THOMAS 2006). *srd-32* belongs to a divergent branch of the SRD phylogeny, which is itself a divergent family of the STR superfamily (ROBERTSON AND THOMAS 2006). *srr-7* belongs to the one of the smallest families of *C. elegans* chemoreceptor

genes, outside of the single opsin family member, *sro-1*, and the *srm* family encoding five chemoreceptor genes (ROBERTSON AND THOMAS 2006)).

seb-3 and *srw-97* exhibited similar enrichment profiles across the CEM neurons, with ~3.5-fold enrichment in CEM VR (**Table 1; Figure 1D; Table S7**). *dmsr-12* showed almost five-fold stronger expression in CEM DL versus other CEM neurons (**Table 1; Figure 1A; Table S8**), while *srd-32* was only 1.62-fold enriched (**Table 1; Figure 1A; Table S8**). *srr-7* showed only two-fold enrichment in CEM VL (**Table 1; Figure 1C; Table S6**), which correlated with previous transcriptomic analyses that found *srr-7* to be enriched in *C. elegans* EVNs (WANG *et al.* 2015).

CEM-specific receptor expression patterns

To confirm our single-cell RNA-seq results, we generated transgenic GFP fusions for the five receptor genes (BOULIN *et al.* 2006). Roughly 3 kb of promoter region upstream of the start codon was included in these constructs, along with the majority of the coding sequence (**Table S10**); this would have automatically included any large 5'-ward introns that might contain cis-regulatory elements of these genes (FUXMAN BASS *et al.* 2014). The GFP coding sequence was cloned from the Fire Kit vector pPD95.75 (BOULIN *et al.* 2006). *pha-1; lite-1; him-5* animals were injected with reporter constructs and the co-injection marker pBX (*pha-1*(+)).We isolated GFP$^+$ strains and imaged and GFP$^+$ males for expression at 63x magnification (**Figure 2; Fig. S1**). An integrated p*pkd-2*::GFP line was used as a CEM-specific control (**Figure 2A**).

The previously characterized GPCR gene, *seb-3*, displayed a non-CEM-specific expression pattern matching that previously described (**Figure 2B**) (JEE *et al.* 2013), and was excluded from further analyses. The other four receptor genes showed transgenic expression patterns similar to their RNA-seq data: GFP-tagged DMSR-12 was heavily enriched in CEM DL, but also exhibited

CEM DR expression, and was observed in both soma and cilia (**Figure 2C**). GFP-tagged SRD-32 was found faintly in both dorsal CEM neurons but exhibited no ciliary localization (**Figure 2D**). GFP-tagged SRW-97 was found in both ventral CEM soma and cilia, with slightly higher expression in CEM VL (**Figure 2E**). GFP-tagged SRR-7 was found in CEM VR, as well as another neuron that is likely to be CEP VR (**Figure 2F**). As with *seb-3*, *srr-7* was excluded from further analyses, as we aimed to identify CEM-specific regulators of the ascr#8 response.

Except for SRD-32, all GFP-tagged receptors showed subcellular localization patterns that included the sensory cilia (**Figure 2, white bars**). Our failure to see this for SRD-32 may be an artifact of our p*srd-32*::GFP construct design, because only 52% of the *srd-32* coding sequence was included in our transgene (**Table S10**).

We also observed non-GPCR genes to be heavily enriched in single CEM neurons, such as *trf-1*, which encodes a TNF receptor homolog (TENOR AND ABALLAY 2008); *trf-1* has an EVN-specific promoter (WANG *et al.* 2015), which provides an alternative to the *pkd-2* and *klp-6* promoters typically used to drive transgenes in EVNs (**Fig. S1**) (PEDEN AND BARR 2005; BAE *et al.* 2006). This fits previous observations of *trf-1*::GFP expression in CEM, HOB, and RnB neurons (WANG *et al.* 2015).

RNAi-mediated knockdown of CEM Receptors

To test whether these CEM-enriched genes encoded receptors that are required in ascr#8 sensation, we used RNAi in a strain that is hypersensitive to neuronal RNA interference, *nre-1; lin-15B* (SCHMITZ *et al.* 2007; POOLE *et al.* 2011). We crossed *nre-1; lin-15B* from this strain into a *him-5* background so that we could assay ascr#8 responses in males. Young adults were then reared on NGM agar plates containing 1 mM IPTG to induce expression of dsRNA

within the food source which would cause receptor-specific RNAi. Young adult males of the subsequent generation were then assayed for their response to ascr#8 after being grown on either a control vector (pL4440) or targeted dsRNA vector.

To confirm that our system for male neuronal RNAi could affect behavioral phenotypes, we first fed animals M02B7.3 (α-*osm-3*) and B0212.5 (α-*osm-9*) RNAi clones from the Ahringer Library (FRASER *et al.* 2000; KAMATH *et al.* 2003). Using our single-worm Spot Retention Assay (NARAYAN *et al.* 2016), we assayed animals subjected to RNAi against *osm-3* or *osm-9* for their behavioral dwell time in ascr#8 (**Figure 3A**). Animals fed *osm-3* dsRNA showed significantly defective responses to ascr#8, like that observed loss-of-function alleles (**Figure 3B**). In contrast, animals fed *osm-9* showed only a slight decrease in their times spent within ascr#8 (**Figure 3A**). Because we could successfully abolish ascr#8 attraction through male neuronal RNAi of *osm-3*, we could be confident that RNAi would be broadly effective at functionally verifying CEM-enriched genes encoding components of the ascr#8 response.

We thus fed animals dsRNA clones targeting three CEM-enriched receptor genes: T18H12.5 (α-*srd-32*), H34P18.1 (α-*dmsr-12*), and ZC204.15 (α-*srw-97*). The α-*srd-32* clone was the only one not available in the Ahringer library (FRASER *et al.* 2000; KAMATH *et al.* 2003), but a clone from the Vidal library was available (RUAL *et al.* 2004). These clones were in the same backbone vector, allowing for the same control vector to be utilized across studies.

RNAi of *srd-32* caused no defect in ascr#8 responses (**Figure 3C**). Either *dmsr-12* or *srw-97* dsRNA caused partial defects of ascr#8 dwell time (**Figure 3C**). Neither knockdown statistically lowered the dwell time in ascr#8 (**Figure 3D**), though they did abolish the statistically significant increase in time spent in ascr#8 over vehicle controls (**Figure 3C**).

CRIPSR-generated null mutants of candidate receptors

We used CRISPR to generate a null allele of *srw-97(knu456)* via InVivo Biosystems and backcrossed it into a *him-5* background for analysis of male attraction to ascr#8. For phenotypic analysis of null mutants, we used our Single Worm Attraction Assay (SWAA) (REILLY *et al.* 2021). In this assay, animals are placed in a well of a 48-well tissue culture plate containing NGM coated in *E. coli* OP50, and either nothing (S), a drop of the vehicle control (V), or the attractive ascaroside (A). The location of animals is recorded over 15 minutes, and the time spent in the center of the well, or cue, is compared (REILLY *et al.* 2021).

Wild-type (*him-5*) animals were strongly attracted to ascr#8 in the SWAA, replicating our previous observations (**Figure 4A, B; Fig. S2**) (REILLY *et al.* 2021). *srw-97(knu456)* males displayed partially defective ascr#8 attraction: their ascr#8 dwell time was no different than that of vehicle (**Figure 4B; Fig. S2**), while their increase over the vehicle was no different than that of *him-5* (**Figure 4A; Fig. S2**).

We were able to restore normal ascr#8 attraction to *srw-97(knu456)* males through transgenesis with a translational fusion construct (p*srw-97*::*srw-97*::GFP) that employed the same promoter as our transcriptional fusion (**Figure 2E**). Expression of the rescue transgene matched that of our initial fusion, with GFP visible in both ventral CEM neurons (**Figure 4C**). Single-worm assays revealed that the *srw-97* rescue construct completely rescued the partial defect in the ascr#8 response (**Figure 4A, B; Fig. S2**).

We obtained a *dmsr-12(tm8706)* null allele from the National BioResource Program in Japan and crossed it into a *him-5* background as well. Like *srw-97(knu456)*, *dmsr-12(tm8706)* males exhibited partially defective responses to ascr#8 (**Figure 5A, B; Fig. S3**). Similarly, the expression profile of the p*dmsr-12*::*dmsr-12*::GFP rescue construct matched its earlier reporter

expression (**Figure 2C, 5C**). This rescue construct also completely restored normal attraction to ascr#8 (**Figure 5A, B; Fig. S3**).

Given that *dmsr-12* is expressed in dorsal CEM neurons, and *srw-97* is expressed in ventral CEM neurons (**Figure 2C, E**), we speculated that single mutants of either *dmsr-12* or *srw-97* partially retained the ability to sense and respond to ascr#8, with the opposing wild-type CEM-specific receptor gene conferring some residual response to ascr#8. We thus generated a *dmsr-12; srw-97* double mutant strain and assayed animals for their ability to respond to ascr#8. These double mutants completely failed to be attracted to or retained by ascr#8 activity (**Figure 5; Fig. S3**). This defect, though strong, was specific to ascr#8 sensation; double mutants showed no defect in their responses to ascr#3 (**Figure 5D, E; Fig. S4**).

Together, these data suggest that at least two GPCR receptors are expressed in opposite pairs of CEM neurons and act in parallel during sensation of ascr#8.

Phylogenetic analyses of ascr#8 receptors reveal likely gene duplication events

The ability to attract mates through pheromones is often essential for a species' survival. However, *C. elegans* is a self-fertile hermaphrodite: male mating is useful in creating genetic diversity but is not absolutely required for species propagation. We have recently observed that different *Caenorhabditis* species show quite different responses to ascr#8 (REILLY *et al.* 2019). To understand this pattern better, we analyzed the evolution of both *srw-97* and *dmsr-12*.

We identified orthologs of *srw-97* from *C. elegans* (*Cel-srw-97*) in other *Caenorhabditis* proteoms via OrthoFinder (**Figure 6A**). A closely related *C. elegans* paralog, *Cel-srw-98*, underwent a species-specific expansion within *C. inopinata*. However, other species, such as *C. briggsae* and *C. nigoni*, have closely related paralogs to *Cel-srw-97*. The coding DNA

sequences (CDS DNAs) of both *Cel-srw-97* and *Cel-srw-98* are 66.2% identical to one another, while their amino acid sequences are only 57.1% identical (MADEIRA *et al.* 2019). In our single-cell CEM RNA-seq data, *Cel-srw-98* shows enrichment similar to that of to *Cel-srw-97*; it is most strongly expressed in CEM VR, although below the two-fold enrichment cutoff that we chose in selecting candidates for functional analysis (**Table 1**).

C. tropicalis, like *C. elegans* and *C. briggsae*, is a hermaphroditic *Caenorhabditis* species for which male mating is optional (NOBLE *et al.* 2021). *C. tropicalis* encodes a reduced number of ascr#8 receptor gene paralogs, with no *Cel-dmsr-12* paralogs, and only one *Cel-srw-97* paralog (**Figure 6**). We previously observed that *C. tropicalis* fails to be attracted to ascr#8, and it is possible that this loss of receptor genes is one reason for that failure (REILLY *et al.* 2019). Given the conserved activity of cis-regulatory elements between different *Caenorhabditis* species (WANG *et al.* 2004; GORDON *et al.* 2015), it would be interesting to express a *Cel-srw-97* construct in *C. tropicalis* to see if it can confer attraction to and retention by ascr#8.

In contrast, the other candidate ascr#8 receptor, *dmsr-12*, does not appear in our phylogenetic analysis to have undergone any species-specific expansion (**Figure 6B**). In fact, outside of *C. elegans*, there are generally fewer paralogs per species. The most closely related *C. elegans* gene in our phylogeny, *Cel-dmsr-13*, does not show CEM enrichment in our single-neuron RNA-seq data, although *Cel-dmsr-10*, *Cel-dmsr-11*, and *Cel-dmsr-16* are somewhat enriched within CEM VR (**Table S7**). Notably, CEM VR is the same neuron in which *srw-97* is enriched.

DISCUSSION

Pheromones are important for mating in many animals. In the nematode *C. elegans*, males are attracted to hermaphrodites as possible mates by the small molecule pheromone ascaroside #8

(PUNGALIYA *et al.* 2009; NARAYAN *et al.* 2016). While the ascaroside class of small molecule pheromones utilized by nematodes is rapidly being elucidated (with over 230 known ascaroside structures so far; *https://smid-db.org*) (ARTYUKHIN *et al.* 2018), the neuronal receptor proteins that mediate pheromone signals remain largely unknown. For only a select few ascarosides have sensory components been identified at the cellular (GREENE *et al.* 2016a; GREENE *et al.* 2016b; CHUTE *et al.* 2019), receptor (KIM *et al.* 2009; MCGRATH *et al.* 2011; PARK *et al.* 2012), or signal transduction levels (ZWAAL *et al.* 1997).

Here, we identify two novel G protein-coupled receptors as active, required components in the sensation and behavioral response to the mating pheromone, ascr#8. Transcripts for the two GPCRs, *dmsr-12* and *srw-97*, are enriched in single CEM neurons (**Table 1**), and they express in non-overlapping subsets of the male-specific chemosensory neurons (**Figure 1, 2**). There are, however, other receptors present in these same neurons that contribute to the navigation of a vast and ever-changing array of environmental cues, such as the widely expressed ethanol sensor, *seb-3* (**Figure 2B**) (JEE *et al.* 2013).

One mechanism for sensory flexibility in CEM neurons may be heterodimerization of receptor proteins. Previous work identified two receptors for ascr#2 in the ASK neuron: DAF-37 and DAF-38 (PARK *et al.* 2012). While both are required for proper ascr#2-induced dauer formation, only DAF-38 is involved in the sensation of other ascarosides (PARK *et al.* 2012). Such heterodimers may also exist for pheromone receptors in CEM neurons.

Another mechanism for sensory flexibility in CEM neurons is to have diverse receptor proteins with distinct specificities co-expressed within a single neuron. Multiple ascarosides are sensed by the male-specific CEM neurons, including ascr#8 and ascr#3 (NARAYAN *et al.* 2016). The two receptors identified here may function as ascr#8-specific receptors, as *dmsr-12;srw-97*

double mutant animals do not exhibit defective responses to ascr#3 (**Figure 5D, E**). The related receptors *dmsr-10*, *dmsr-13*, *dmsr-16*, and *srw-98* are enriched in ventral CEM neurons, and may heterodimerize with *srw-97*, to result in fine-tuned sensation of ascr#8. Similarly, there may be other receptors may be enriched in the dorsal CEM neurons to heterodimerize with *dmsr-12*. The role of DAF-37 as an ascr#2-specific receptor further supports our hypothesis, as *dmsr-12* is related to DAF-37 (ROBERTSON AND THOMAS 2006). The ventral CEM-receptor, *srw-97* falls within the same large family of GPCRs as well (KRISHNAN *et al.* 2014), while the promiscuous DAF-38 does not (ROBERTSON AND THOMAS 2006).

The initial goal of our single-cell RNA-seq analysis of male-specific chemosensory CEM neurons was to identify GPCRs encoding pheromone receptors. However, further analysis of other genes with CEM-enriched expression should also uncover specific and novel promoter profiles, which will enable optogenetic manipulation and calcium imaging of defined individual CEM neurons (NARAYAN *et al.* 2016). The development of advanced transgenic reagents will also permit chemical biology of CEM neurons. We have recently developed an active ascr#8 bioaffinity probe to employ in the targeted elucidation of ascr#8 receptors (ZHANG *et al.* 2019). Use of this probe will lead to further elucidation of the identity of acsr#8 receptors, by confirming either SRW-97 or DMSR-12 as receptors or identifying their heterodimeric partners. The combination of these technologies should clarify how heterogeneous CEM neurons achieve homogeneous sensory responses.

METHODS

Single cell isolation and RT-PCR

Microdissection and single-cell RT-PCR of individual CEM_DL, CEM_DR, CEM_VL, and CEM_DR neurons was performed essentially as described (SCHWARZ *et al.* 2012). For all four neuronal types, single-end 50-nucleotide (nt) RNA-seq was performed on an Illumina HiSeq 2000. To identify so-called housekeeping genes and genes primarily active outside the nervous system, we compared our results from CEM_DL, CEM_DR, CEM_VL, and CEM_DR to equivalent analyses of published single-end 38-nt RNA-seq data from mixed-stage whole *C. elegans* hermaphrodite larvae (SCHWARZ *et al.* 2012).

Transcriptional analysis

Reads were quality-filtered as follows: neuronal reads that failed Chastity filtering were discarded (Chastity filtering had not been available for the larval reads); raw 38-nt larval reads were trimmed 1 nt to 37 nt; all reads were trimmed to remove any indeterminate ("N") residues or residues with a quality score of less than 3; and larval reads that had been trimmed below 37 nt were deleted, as were neuronal reads that had been trimmed below 50 nt. This left a total ranging from 21,554,964 (CEM_VL) to 24,546,096 (CEM_DL) filtered reads for analysis of each neuronal type, versus 23,369,056 filtered reads for whole larvae (**Table S2**).

We used RSEM version 1.2.17 (LI AND DEWEY 2011) with bowtie2 version 2.2.3 (LANGMEAD AND SALZBERG 2012) and SAMTools version 1.0 (LI *et al.* 2009) to map filtered reads to a *C. elegans* gene index and generate read counts and gene expression levels in transcripts per million (TPM). To create the *C. elegans* gene index, we ran RSEM's *rsem-prepare-reference* with the arguments '*--bowtie2 --transcript-to-gene-map*' upon a collection of coding DNA sequences

(CDSes) from both protein-coding and non-protein-coding *C. elegans* genes in WormBase release WS245 (HOWE *et al.* 2016). The CDS sequences were obtained from *ftp://ftp.sanger.ac.uk/pub2/wormbase/releases/WS245/species/c_elegans/PRJNA13758/c_elegans.PRJNA13758.WS245.mRNA_transcripts.fa.gz* and *ftp://ftp.sanger.ac.uk/pub2/wormbase/releases/WS245/species/c_elegans/PRJNA13758/c_elegans.PRJNA13758.WS245.ncRNA_transcripts.fa.gz*. For each RNA-seq data set of interest, we computed mapped reads and expression levels per gene by running RSEM's *rsem-calculate-expression* with the arguments '*--bowtie2 -p 8 --no-bam-output --calc-pme --calc-ci --ci-credibility-level 0.99 --fragment-length-mean 200 --fragment-length-sd 20 --estimate-rspd --ci-memory 30000*'. These arguments, in particular '*--estimate-rspd*', were aimed at dealing with single-end data from 3'-biased RT-PCR reactions; the arguments '*--phred33-quals*' and '*--phred64-quals*' were also used for the neuronal and larval reads, respectively. We computed posterior mean estimates (PMEs) both for read counts and for gene expression levels, and rounded PMEs of read counts down to the nearest lesser integer. We also computed 99% credibility intervals (CIs) for expression data, so that we could use the minimum value in the 99% CI for TPM as a robust minimum estimate of a gene's expression (minTPM).

We observed the following overall alignment rates of the reads to the WS245 *C. elegans* gene index: 48.01% for the CEM_DL read set, 28.19% for the CEM_DR read set, 40.75% for the CEM_VL read set, 19.73% for the CEM_VR read set, and 76.41% for the larval read set (**Table S2**). A similar discrepancy between lower alignment rates for hand-dissected linker cell RNA-seq reads versus higher alignment rates for whole larval RNA-seq reads was previously observed, and found to be due to a much higher rate of human contaminant RNA sequences in the hand-dissected linker cells (SCHWARZ *et al.* 2012). We defined detectable expression for a gene in a given

RNA-seq data set by that gene having an expression level of 0.1 TPM; we defined robust expression by that gene having a minimum estimated expression level (termed minTPM) of at least 0.1 TPM in a credibility interval of 99% (i.e., ≥ 0.1 minTPM). The numbers of genes being scored as expressed in a given neuronal type above background levels, for various data sets, are given in **Table S3**. Other results from RSEM analysis are given in **Table S3**.

We annotated *C. elegans* genes and the encoded gene products in several ways (**Table S5**). For the products of protein-coding genes, we predicted classical signal and transmembrane sequences with Phobius 1.01 (KÄLL *et al.* 2004), regions of low sequence complexity with pseg (SEG for proteins, from *ftp://ftp.ncbi.nlm.nih.gov/pub/seg/pseg*) (WOOTTON 1994), and coiled-coil domains with ncoils (from *http://www.russell.embl-heidelberg.de/coils/coils.tar.gz*) (LUPAS 1996). PFAM 27.0 protein domains from PFAM (FINN *et al.* 2016) were detected with HMMER 3.0/hmmsearch (EDDY 2009) at a threshold of $E \leq 10^{-5}$. The memberships of genes in orthology groups from eggNOG 3.0 (POWELL *et al.* 2012) were extracted from WormBase WS245 with the TableMaker function of ACEDB 4.3.39. Genes with likely housekeeping status (based on ubiquitous expression in both larvae and linker cells) were as identified in our previous work (SCHWARZ *et al.* 2012). Genes were predicted to encode GPCRs on the basis of their encoding a product containing one or more of the following Pfam-A protein domains: 7tm_1 [PF00001.16], 7tm_2 [PF00002.19], 7tm_3 [PF00003.17], 7tm_7 [PF08395.7], 7TM_GPCR_Srab [PF10292.4], 7TM_GPCR_Sra [PF02117.11], 7TM_GPCR_Srbc [PF10316.4], 7TM_GPCR_Srb [PF02175.11], 7TM_GPCR_Srd [PF10317.4], 7TM_GPCR_Srh [PF10318.4], 7TM_GPCR_Sri [PF10327.4], 7TM_GPCR_Srj [PF10319.4], 7TM_GPCR_Srsx [PF10320.4], 7TM_GPCR_Srt [PF10321.4], 7TM_GPCR_Sru [PF10322.4], 7TM_GPCR_Srv [PF10323.4], 7TM_GPCR_Srw [PF10324.4], 7TM_GPCR_Srx [PF10328.4], 7TM_GPCR_Srz [PF10325.4], 7TM_GPCR_Str

[PF10326.4], ABA_GPCR [PF12430.3], Sre [PF03125.13], and Srg [PF02118.16]. By this criterion, we identified 1,615 genes encoding GPCRs in the WS245 version of the *C. elegans* genome; this resembles a previous estimate of ~1,470 *C. elegans* genes encoding chemoreceptors and other GPCRs, identified through extensive computational and manual analysis (HOBERT 2013). The memberships of genes in orthology groups from eggNOG 3.0 (POWELL *et al.* 2012) were extracted directly from WormBase WS245 with the TableMaker function of ACEDB 4.3.39. Genes with likely housekeeping status (based on ubiquitous expression in both larvae and linker cells) were as identified in our previous work (SCHWARZ *et al.* 2012). Gene Ontology (GO) annotations for *C. elegans* genes were extracted from WormBase-computed annotations in *ftp://ftp.wormbase.org/pub/wormbase/releases/WS245/ONTOLOGY/gene_association.WS245.wb.c_elegans*; human-readable text descriptions for GO term IDs were extracted from *term.txt* in the Gene Ontology archive *http://archive.geneontology.org/full/2014-07-01/go_201407-termdb-tables.tar.gz*.

GFP reporter construction

Reporter fusion constructs were generated using previously described techniques (BOULIN *et al.* 2006). Approximately 2-3 kb of upstream promoter region of each gene was included in construct generation, as well as a portion of the coding sequence (**Table S10**). This was then fused to GFP (from the Fire Vector Kit plasmid, pPD95.75), via PCR fusion (BOULIN *et al.* 2006). Primers were designed using Primer 3 and ordered from IDT (Integrated DNA Technologies). Primer sequences available in **Table S12**. Successful fusion was confirmed via gel electrophoresis prior to injection.

Reporter fusion constructs were injected into the gonads of *pha-1(e2123ts); lite-1(ce314); him-5(e1490)* animals, along with a co-injection marker of pBX(*pha-1*(+)). In this manner, positive array animals will propagate normally at 20 °C. Strains were confirmed via GFP expression, with multiple array lines being generated per injection (**Table S11**). Injections were performed by InVivo Biosystems, with strain isolation being performed in house.

Imaging

Animals were imaged for GFP expression using previously described techniques. GFP+ young adult male animals were mounted on a 1% agarose pad and immobilized with sodium azide. Animals were then imaged on a spinning disk confocal microscope at 63x magnification. Z-stack imaging was performed, generating 3D reconstructions of the heads of the imaged animals. Central/optimal z-plane images were used to generate the images used to verify expression (**Figure 2; Fig. S1**).

RNAi Feeding

VH624 (*rhIs13* [*unc-119*::GFP + *dpy-20*(+)]; *nre-1(hd20)*; *lin-15B(hd126)*) animals (SCHMITZ *et al.* 2007; POOLE *et al.* 2011) were crossed with *him-5(e1490)* animals to integrate male production into a strain hypersensitive to neuronal RNAi-knockdown, generating JSR44 (*nre-1(hd20)*; *lin-15B(hd126); him-5(e1490)*). During the cross, insertion of the *him-5(e1490)* allele displaced the integrated array *rhIs13*, suggesting location of the array on Chromosome V. Presence of *lin-15B(hd126)* in JSR44 was confirmed via sequencing. The non-annotated *nre-1(hd20)* is linked with *lin-15B*, being retained alongside *lin-15B* (SCHMITZ *et al.* 2007; POOLE *et al.* 2011).

RNAi clones were grown overnight in cultures of LB containing 50 µg/mL ampicillin. Cultures were then diluted to an OD_{600} of 1.0 before plating on NGM agar plates containing 50 µg/mL ampicillin and 1 mM IPTG (Isopropyl-β-D-thiogalactoside) to select for RNAi clones and induce expression. Lawns were allowed to grow at room temperature for 8-16 hours, before JSR44 young adult hermaphrodites were placed on the plates and left to propagate at 16°C. Young adult males of the F1 progeny were then selected for behavioral testing suing the *Spot Retention Assay*. Empty vector controls (VC-1 clone) were run alongside every targeted knockdown experiment.

Spot Retention Assay

Following previously described methods, young adult males were isolated from hermaphrodites 5-16 hours prior to testing (PUNGALIYA *et al.* 2009; NARAYAN *et al.* 2016). In short, at the time of the assay, 0.6 µL of either vehicle control (-) or ascaroside #8 (+) was added to the NGM plates covered in a thin lawn of OP50 *E. coli*. Ten males were then divided between two pre-marked spots on the agar, equidistant from the cues. The plate was then recorded for 20 minutes. The time spent of each visit in either vehicle or ascaroside #8 (if greater than 10 seconds) was scored, and averaged. Plates in which the average was greater than two standard deviations removed from the population average were removed from the final analysis as outliers. To compare between strains or conditions, the vehicle was subtracted from the ascaroside dwell time for each plate. The average of these differences was then compared statistically.

Single Worm Behavioral Assay

Following previously described methods (PUNGALIYA *et al.* 2009; NARAYAN *et al.* 2016; REILLY *et al.* 2021), animals were isolated and prepared in an identical manner to the Spot

Retention Assay. The two outside rings of wells in a 48-well tissue culture plate were filled with 200 µL of NGM agar, which was then seeded with 65 µL of OP50 *E. coli*. The plates and lawns were then dried at 37 °C for 4 hours. Alternating wells were then prepared as spatial controls (nothing done), vehicle controls (0.85 µL of dH_2O was placed in the center of the well), or ascaroside well (0.85 µL of ascaroside was placed in the center of the well). This was performed over four quadrants. Animals were scored for their visits and duration to the center of the well and/or the cue.

The average duration of each worm's visits was calculated, and these values were again averaged together to generate a Mean Dwell Time in seconds for each plate. When comparing across strains or conditions, the Spatial controls were then compared for statistical difference. If none was observed, the Log(fold-change) A/V was then calculated by taking the log of the ascaroside mean dwell time divided by the vehicle mean dwell time for each plate. The amount of times each worm visited the center was averaged to generate the Visit Counts.

The Percent Attraction values were calculated by first determining the "attractive" cut off as two standard deviations above the vehicle average. Any visit longer than this was deemed "attractive" and scored as a "1"; non-attractive visits were scored as "0". The percent attraction was then calculated for each worm was the percent of visits scored a "1". The average was then calculated across the plate to determine Percent Attraction.

CRISPR Design and Strain Generation

A novel null mutation was generated for *srw-97* by InVivo Biosystems. The *srw-97(knu456)* allele was generated in a *him-5(e1490)* strain using two sgRNAs (TTTAGTAGAGCAGAAATTAA and TACAGCTTTAACTTTCAAC) to generate a 1,620-nt

deletion which removed the start codon and left only the terminal exon intact. The *knu456* knockout allele was generated by donor homology using the pNU1361odn oligo: (TTTTCTTGTATTTCCAAAAATTGTAAAAACCTTTATGAAAGTTAAAGCTGTAAGGAT TTTCAGACATTTA). Following generation of a homozygous deletion by InVivo Biosystems, the line was then backcrossed twice into *him-5(e1490)*.

The *dmsr-12(tm8706)* allele, provided by the National BioResource Group (NRBP) contains a 118-nucleotide deletion that was generated by Dr. Mitani of the NRBP. The allele was crossed into a *him-5(e1490)* background prior to testing. The deletion spans intron 2 and exon 3 of the coding sequence. Whether this results in a correctly spliced gene remains unknown, although the expected remaining coding sequence remains in frame.

Phylogenetic Analyses

For phylogenetic analysis of selected CEM genes, we downloaded proteomes for *C. elegans* and related *Caenorhabditis* nematodes from WormBase (release WS275), the Blaxter *Caenorhabditis* database (release 1), or our unpublished work, as listed in **Table S4**. From each proteome, we extracted the longest predicted isoform for each gene with *get_largest_isoforms.pl* (*https://github.com/SchwarzEM/ems_perl/blob/master/fasta/get_largest_isoforms.pl*). We observed that the predicted isoform for *dmsr-12* in the WormBase WS275 release of *C. elegans*' proteome was shorter than past versions of *dmsr-12*, and that the WS275 isoform omitted exons that our transgenic expression data (based on older gene models for *dmsr-12*) indicated were likely to be real. We therefore manually replaced the WS275 version of *dmsr-12* with an older version (extracted from the *C. elegans* proteome in the WS250 release of WormBase). We then computed orthology groups for *C. elegans* and its related species with OrthoFinder version 2.3.11 (EMMS

AND KELLY 2015; EMMS AND KELLY 2019), using the arguments '*-a 1 -S diamond -og*'. We identified which orthology groups contained the *C. elegans* genes *srr-7*, *srw-97*, and *dmsr-12*, and extracted their sequences from a concatenation of all 11 proteomes via *extract_fasta_subset.pl* (*https://github.com/SchwarzEM/ems_perl/blob/master/fasta/extract_fasta_subset.pl*). For each orthogroup's member sequences, we aligned the sequences with MAFFT version 7.455 (KATOH AND STANDLEY 2013) and filtered the alignments twice with trimAl version 1.4.rev15 (CAPELLA-GUTIÉRREZ *et al.* 2009), using first the argument '*-automated1*' and then the arguments '*-resoverlap 0.50 -seqoverlap 50*'. From the filtered alignments, we computed maximum-likelihood protein phylogenies with IQ-TREE version 2.0-rc1 (NGUYEN *et al.* 2015; KALYAANAMOORTHY *et al.* 2017), using the arguments '*-m MFP -b 100 --tbe*'. In particular, we used transfer bootstrap expectation ('*--tbe*') which provides more reliable confidence values than classic bootstrapping (LEMOINE *et al.* 2018). We visualized the resulting phylogenies with FigTree version 1.4.4 (*http://tree.bio.ed.ac.uk/software/figtree*).

Statistical Analyses

Prior to any statistical analyses, outliers were identified and removed. Outliers were defined as any data points greater than two standard deviations removed from the average. All data were then tested for normality using a Shapiro-Wilk Normality Test. This test was chosen over the more conventional D'Agostino-Pearson Normality Test as many data sets were below 10 in number (due to the statistical power offered by the Single Worm Behavioral Assay (REILLY *et al.* 2021).

The Spot Retention Assay data was analyzed using paired *t*-tests or Wilcoxon Matched-Pairs Signed Rank tests to compare vehicle control and ascaroside dwell times within strains

following tests for normality (**Figure 3**). When comparing the values of multiple conditions or strains, the data was first normalized to account for vehicle dwell time variation between plates using a base-2 exponentiation, as described previously, to transform all data points into non-zero values. This allows for the calculation of the fold-change as the log(base2) of the ascaroside dwell time divided by the vehicle dwell time. These normalized values were then compared using a Mann-Whitney test or a One-Way ANOVA followed by a Dunnett's multiple comparisons test (**Figure 3**).

The Single Worm Behavioral Assay was first analyzed within each strain by performing either a Repeated-Measures ANOVA followed by a Dunnett's multiple comparisons test or Friedman test followed by Dunn's correction, comparing both Spatial control and Ascaroside dwell times to that of the Vehicle Control. The log(fold-change) of raw ascaroside and vehicle dwell time values were calculated and compared using either a One-Way ANOVA followed by a Bonferroni's multiple corrections test or Friedman Test followed by Dunn's correction (**Figure 4, 5**). The ascr#3 log(fold-change) values were compared using a Student's *t*-test (**Figure 5E**). Visit Counts were compared in the same manner as the Mean Dwell Time data, while the Percent Attraction data was analyzed using paired *t*-tests or Wilcoxon Matched-Pairs Signed Rank tests to compare the attractive values of the vehicle and ascaroside (**Figures S2, S3, S4**).

Data availability

RNA-seq reads will be submitted to the Sequence Read Archive (SRA; *https://www.ncbi.nlm.nih.gov/sra*).

ACKNOWLEDGEMENTS

We thank the *Caenorhabditis* Genetics Center, which is funded by the NIH Office of Research Infrastructure Programs (P40 OD01044), as well as the National BioResource Project, L. Rene Garcia (Texas A&M University), and Douglas Portman (University of Rochester Medical Center) for providing strains. We also thank InVivo Biosystems for generating transgenic and CRISPR knockout animals. The synthetic ascr#8 utilized in this study was provided by Frank Schroeder (Cornell University). The research reported in this publication was supported by NIH R01 DC016058 (J.S.), R01 GM084389 (P.W.S.), the Howard Hughes Medical Institute (P.W.S.), Moore Foundation Grant No. 4551 (E.M.S.), and Cornell startup funding (E.M.S.). We thank Titus Brown and the Michigan State University High-Performance Computing Center (supported by U.S. Department of Agriculture grant 2010-65205-20361 and NIFA–National Science Foundation (NSF) grant IOS-0923812) for computational support; additional computing was enabled by start-up and research allocations from NSF XSEDE (TG-MCB180039 and TG-MCB190010).

588 **FIGURE AND TABLE LEGENDS**

Gene	CEM DL	CEM DR	CEM VL	CEM VR	Max CEM
pkd-2	1.30	0.09	0.25	0.77	143
seb-3	0.15	0.31	0.23	**3.25**	6.50
dmsr-12	**4.96**	0.06	0.04	0.11	4.96
srd-32	**1.62**	0.38	0.23	0.62	4.33
srw-97	0.14	0.27	0.18	**3.67**	5.50
srr-7	0.16	0.26	**1.90**	0.53	6.33
trf-1	0.00	0.00	0.00	226.28	226.28

589 **Table 1. Enrichment levels of candidate GPCR genes in CEM neurons.** Enrichment levels
590 displayed as normalized count within a single CEM cell type over the normalized count in the
591 remaining three CEM neurons. Max CEM is the enrichment in all four CEM neurons over the
592 remainder of the animal. The CEM with highest enrichment of each GPCR gene are denoted by
593 bolded-underlined values.

594

595 **Figure 1. Transcriptomic landscapes of the CEM neurons. (A-D)** TPKM plots of individual
596 CEM DL **(A)**, CEM DR **(B)**, CEM VL **(C)**, and CEM VR **(D)** neurons. X-axes display enrichment
597 in individual CEM neurons compared to whole larvae, while the Y-axes display total transcript
598 counts (TPM). Genes of interest are denoted by colored symbols, defined in the legend.

599

600 **Figure 2. Expression profiles of CEM-enriched GPCR genes of interest.** Transcriptional GFP
601 fusions of GPCR genes enriched in the CEM neurons. **(A)** A previously published CEM reporter,
602 p*pkd-2*::GFP. **(B)** p*seb*-3::GFP, matching previously published expression, with no discernable
603 enrichment in the CEM. **(C)** p*dmsr-12*::GFP is strongly expressed in the CEM DL neuron, as well
604 as the CEM DR soma. **(D)** p*srd-32*::GFP is weakly expressed in the somas of CEM DR and DL.
605 **(E)** p*srw-97*::GFP is expressed in both CEM VR and VL, with localization in the cilia as well as

606 the soma. **(F)** p*srr-7*::GFP is expressed in CEM VR, both the soma and cilia, as well the cilial of
607 a neighboring neuron, presumably CEP VR. Dorsal/ventral axes and anterior/posterior directions
608 shown in (B). Scale bars denote distal, cilia region.
609
610 **Figure 3. Knockdown of CEM-enriched GPCR candidates results in aberrant behavioral**
611 **response to ascr#8. (A)** Raw dwell times and **(B)** Log2(fold-change of ascr#8/vehicle) of RNAi
612 knockdown of the kinesin motor, *osm-3*, and the TRPV channel, *osm-9* confirm the ability of RNAi
613 feeding to affect pheromone-driven behaviors in a targeted manner. $n \geq 5$. **(C)** Raw dwell times
614 and **(D)** Log2(fold-change) of genetic null *osm-3* mutants reveal an inability to respond to ascr#8.
615 $n \geq 17$. **(E)** Raw dwell time and **(F)** Log2(fold-change) of GPCR of interest (*srd-32*, *dmsr*-12, and
616 *srw-97*) knockdown reveals *dmsr-12* and *srw-97* as contributors to the ascr#8 behavioral response.
617 $n \geq 4$. Error bars denote SEM. **(A, C, E)** Paired *t*-tests and Wilcoxon tests of vehicle control versus
618 ascr#8 dwell time, **(B)** ANOVA, followed by Bonferroni post-hoc tests comparing Log2(fold-
619 change) of RNAi knockdowns to VC-1 control and to each other, **(D)** Mann-Whitney test
620 comparing *him-5* and *osm-3* Log2(fold-change) in response to ascr#8, **(F)** ANOVA, followed by
621 Dunnett's post-hoc test comparing Log2(fold-change) of RNAi knockdowns to VC-1 control. * p
622 < 0.05, ** $p < 0.01$, **** $p < 0.0001$.
623
624 **Figure 4. The GPCR, SRW-97, is involved in the ascr#8 behavioral response. (A)** Raw dwell
625 times and **(B)** Log(fold-change) of *srw-97* knockout and transgenic rescue (WorEx57) animals.
626 **(C)** Expression of WorEx57 (p*srw-97*::*srw-97*::GFP) in CEM VR. Anterior/Posterior and
627 Right/Left axes denoted. Error bars denote SEM. $n \geq 5$. **(A)** ANOVA followed by Dunnett's post-

hoc test or Friedman test followed by Dunn's (within strain), **(B)** Friedman test, followed by Dunn's post-hoc test (between strain log(fold-change) values). * $p < 0.05$, ** $p < 0.01$.

Figure 5. The DMSR-12 receptor acts in non-SRW-97-expressing CEM neurons to aid in driving the ascr#8 response. **(A)** Raw dwell times and **(B)** Log(fold-change) of *dmsr-12* knockout and transgenic rescue (WorEx54) animals. **(C)** Expression of WorEx54 (p*dmsr-12*::*dmsr-12*::GFP) in CEM DL and CEM DR. Anterior/Posterior and Dorsal/Ventral axes denoted. **(D)** Raw dwell times and **(F)** Log(fold-change) of *him-5* and *dmsr-12;srw-97* animals in response to the structurally related attracted pheromone, ascr#3. **(E)** Structural comparison of ascr#8 (top) and ascr#3 (bottom). Error bars denote SEM. $n \geq 5$. **(A, D)** ANOVA followed by Dunnett's post-hoc test or Friedman test followed by Dunn's post-hoc test (within strain), **(B)** ANOVA, followed by Bonferroni post-hoc test (between strain log(fold-change) values), **(F)** Student's t-test between strain log(fold-change) values. * $p < 0.05$.

Figure 6. Phylogenetic analysis of ascr#8-receptor candidate paralogs across the *Caenorhabditis* genus. (A) The phylogeny of *Cel_srw-97* reveals a *C. inopinata*-specific amplification of *Cel_srw-98*. **(B)** The phylogeny of *Cel_dmsr-12* shows conserved counts of orthologs across the genus. Genes for *C. elegans* denoted in purple; *C. inopinata* in pink, *C. nigoni* in light blue, *C. briggsae* in dark blue, *C. japonica* in red, and *C. tropicalis* in dark green. Distance reference bars (0.1) depict substitutions per site.

REFERENCES

Apirson, E. Z., and I. Ruvinsky, 2019a Coordinated behavioral and physiological responses to a social signal are regulated by a shared neuronal circuit. Curr Biol.

Apirson, E. Z., and I. Ruvinsky, 2019b Dynamic regulation of adult-specific functions of the nervous system by signaling from the reproductive system. Curr Biol.

Aprison, E. Z., and I. Ruvinsky, 2015 Sex Pheromones of *C. elegans* Males Prime the Female Reproductive System and Ameliorate the Effects of Heat Stress. PLoS Genet 11**:** e1005729.

Aprison, E. Z., and I. Ruvinsky, 2017 Counteracting Ascarosides Act through Distinct Neurons to Determine the Sexual Identity of *C. elegans* Pheromones. Curr Biol 27**:** 2589-2599.e2583.

Artyukhin, A. B., Y. K. Zhang, A. E. Akagi, O. Panda, P. W. Sternberg *et al.*, 2018 Metabolomic "Dark Matter" Dependent on Peroxisomal beta-Oxidation in *Caenorhabditis elegans*. J Am Chem Soc 140**:** 2841-2852.

Bae, Y. K., H. Qin, K. M. Knobel, J. Hu, J. L. Rosenbaum *et al.*, 2006 General and cell-type specific mechanisms target TRPP2/PKD-2 to cilia. Development 133**:** 3859-3870.

Boulin, T., J. F. Etchberger and O. Hobert, 2006 Reporter gene fusions. WormBook**:** 1-23.

Butcher, R. A., 2017 Small-molecule pheromones and hormones controlling nematode development. Nat Chem Biol 13**:** 577-586.

Butcher, R. A., M. Fujita, F. C. Schroeder and J. Clardy, 2007 Small-molecule pheromones that control dauer development in *Caenorhabditis elegans*. Nat Chem Biol 3**:** 420-422.

Butcher, R. A., J. R. Ragains and J. Clardy, 2009 An indole-containing dauer pheromone component with unusual dauer inhibitory activity at higher concentrations. Org Lett 11**:** 3100-3103.

671 Butcher, R. A., J. R. Ragains, E. Kim and J. Clardy, 2008 A potent dauer pheromone component
672 in Caenorhabditis elegans that acts synergistically with other components. Proc Natl Acad
673 Sci U S A 105**:** 14288-14292.
674 Capella-Gutiérrez, S., J. M. Silla-Martínez and T. Gabaldón, 2009 trimAl: a tool for automated
675 alignment trimming in large-scale phylogenetic analyses. Bioinformatics (Oxford,
676 England) 25**:** 1972-1973.
677 Choe, A., S. H. von Reuss, D. Kogan, R. B. Gasser, E. G. Platzer *et al.*, 2012 Ascaroside Signaling
678 is Widely Conserved Among Nematodes. Current Biology 22**:** 772-780.
679 Chute, C. D., E. M. DiLoreto, Y. K. Zhang, D. K. Reilly, D. Rayes *et al.*, 2019 Co-option of
680 neurotransmitter signaling for inter-organismal communication in *C. elegans*. Nat
681 Commun 10**:** 3186.
682 Cochella, L., B. Tursun, Y. W. Hsieh, S. Galindo, R. J. Johnston *et al.*, 2014 Two distinct types of
683 neuronal asymmetries are controlled by the *Caenorhabditis elegans* zinc finger
684 transcription factor die-1. Genes Dev 28**:** 34-43.
685 Dong, C., F. Dolke and S. H. von Reuss, 2016 Selective MS screening reveals a sex pheromone in
686 Caenorhabditis briggsae and species-specificity in indole ascaroside signalling. Org
687 Biomol Chem 14**:** 7217-7225.
688 Dong, C., D. K. Reilly, C. Bergame, F. Dolke, J. Srinivasan *et al.*, 2018 Comparative Ascaroside
689 Profiling of *Caenorhabditis* Exometabolomes Reveals Species-Specific (ω) and (ω - 2)-
690 Hydroxylation Downstream of Peroxisomal beta-Oxidation. J Org Chem.
691 Eddy, S. R., 2009 A new generation of homology search tools based on probabilistic inference.
692 Genome informatics. International Conference on Genome Informatics 23**:** 205-211.

693 Emms, D. M., and S. Kelly, 2015 OrthoFinder: solving fundamental biases in whole genome
694 comparisons dramatically improves orthogroup inference accuracy. Genome Biology 16**:**
695 157.
696 Emms, D. M., and S. Kelly, 2019 OrthoFinder: phylogenetic orthology inference for comparative
697 genomics. Genome Biology 20**:** 238.
698 Fagan, K. A., J. Luo, R. C. Lagoy, F. C. Schroeder, D. R. Albrecht *et al.*, 2018 A Single-Neuron
699 Chemosensory Switch Determines the Valence of a Sexually Dimorphic Sensory Behavior.
700 Curr Biol 28**:** 902-914.e905.
701 Finn, R. D., P. Coggill, R. Y. Eberhardt, S. R. Eddy, J. Mistry *et al.*, 2016 The Pfam protein
702 families database: towards a more sustainable future. Nucleic acids research 44**:** D279-
703 D285.
704 Fraser, A. G., R. S. Kamath, P. Zipperlen, M. Martinez-Campos, M. Sohrmann *et al.*, 2000
705 Functional genomic analysis of *C. elegans* chromosome I by systematic RNA interference.
706 Nature 408**:** 325-330.
707 Fuxman Bass, J. I., A. M. Tamburino, A. Mori, N. Beittel, M. T. Weirauch *et al.*, 2014
708 Transcription factor binding to Caenorhabditis elegans first introns reveals lack of
709 redundancy with gene promoters. Nucleic Acids Res 42**:** 153-162.
710 Gene Ontology, C., 2021 The Gene Ontology resource: enriching a GOld mine. Nucleic acids
711 research 49**:** D325-D334.
712 Goodman, M. B., D. H. Hall, L. Avery and S. R. Lockery, 1998 Active currents regulate sensitivity
713 and dynamic range in *C. elegans* neurons. Neuron 20**:** 763-772.

714 Gordon, K. L., R. K. Arthur and I. Ruvinsky, 2015 Phylum-Level Conservation of Regulatory
715 Information in Nematodes despite Extensive Non-coding Sequence Divergence. PLoS
716 genetics 11**:** e1005268-e1005268.
717 Greene, J. S., M. Brown, M. Dobosiewicz, I. G. Ishida, E. Z. Macosko *et al.*, 2016b Balancing
718 selection shapes density-dependent foraging behaviour. Nature 539**:** 254-258.
719 Greene, J. S., M. Dobosiewicz, R. A. Butcher, P. T. McGrath and C. I. Bargmann, 2016a
720 Regulatory changes in two chemoreceptor genes contribute to a *Caenorhabditis elegans*
721 QTL for foraging behavior. Elife 5.
722 Harris, T. W., V. Arnaboldi, S. Cain, J. Chan, W. J. Chen *et al.*, 2020 WormBase: a modern Model
723 Organism Information Resource. Nucleic Acids Res 48**:** D762-d767.
724 Hobert, O., 2013 The neuronal genome of *Caenorhabditis elegans*. WormBook**:** 1-106.
725 Houck, L., C. Palmer, R. Watts, S. Arnold, P. Feldhoff *et al.*, 2007 A new vertebrate courtship
726 pheromone, PMF, affects female receptivity in a terrestrial salamander. Animal Behaviour
727 73**:** 315-320.
728 Howe, K. L., B. J. Bolt, S. Cain, J. Chan, W. J. Chen *et al.*, 2016 WormBase 2016: expanding to
729 enable helminth genomic research. Nucleic acids research 44**:** D774-D780.
730 Hrus, A., G. Lau, H. Hutter, S. Schenk, J. Ferralli *et al.*, 2007 *C. elegans* Agrin Is Expressed in
731 Pharynx, IL1 Neurons and Distal Tip Cells and Does Not Genetically Interact with Genes
732 Involved in Synaptogenesis or Muscle Function. PLOS ONE 2**:** e731.
733 Jang, Y. H., H. S. Chae and Y. J. Kim, 2017 Female-specific myoinhibitory peptide neurons
734 regulate mating receptivity in *Drosophila melanogaster*. Nat Commun 8**:** 1630.

735 Jee, C., J. Lee, J. P. Lim, D. Parry, R. O. Messing *et al.*, 2013 SEB-3, a CRF receptor-like GPCR,
736 regulates locomotor activity states, stress responses, and ethanol tolerance in *C. elegans*.
737 Genes, brain, and behavior 12**:** 10.1111/j.1601-1183X.2012.00829.x.
738 Kaletsky, R., V. Lakhina, R. Arey, A. Williams, J. Landis *et al.*, 2016 The C. elegans adult
739 neuronal IIS/FOXO transcriptome reveals adult phenotype regulators. Nature 529**:** 92-96.
740 Käll, L., A. Krogh and E. L. L. Sonnhammer, 2004 A combined transmembrane topology and
741 signal peptide prediction method. Journal of molecular biology 338**:** 1027-1036.
742 Kalyaanamoorthy, S., B. Q. Minh, T. K. F. Wong, A. von Haeseler and L. S. Jermiin, 2017
743 ModelFinder: fast model selection for accurate phylogenetic estimates. Nature methods
744 14**:** 587-589.
745 Kamath, R. S., A. G. Fraser, Y. Dong, G. Poulin, R. Durbin *et al.*, 2003 Systematic functional
746 analysis of the *Caenorhabditis elegans* genome using RNAi. Nature 421**:** 231-237.
747 Katoh, K., and D. M. Standley, 2013 MAFFT multiple sequence alignment software version 7:
748 improvements in performance and usability. Molecular biology and evolution 30**:** 772-780.
749 Kim, K., K. Sato, M. Shibuya, D. M. Zeiger, R. A. Butcher *et al.*, 2009 Two Chemoreceptors
750 Mediate Developmental Effects of Dauer Pheromone in *C. elegans*. Science 326**:** 994-998.
751 Krishnan, A., M. S. Almén, R. Fredriksson and H. B. Schiöth, 2014 Insights into the Origin of
752 Nematode Chemosensory GPCRs: Putative Orthologs of the Srw Family Are Found across
753 Several Phyla of Protostomes. PLoS ONE 9**:** e93048.
754 Langmead, B., and S. L. Salzberg, 2012 Fast gapped-read alignment with Bowtie 2. Nature
755 methods 9**:** 357-359.

Lee, H., M.-k. Choi, D. Lee, H.-s. Kim, H. Hwang *et al.*, 2012 Nictation, a dispersal behavior of the nematode Caenorhabditis elegans, is regulated by IL2 neurons. Nature Neuroscience 15**:** 107-112.

Lemoine, F., J. B. Domelevo Entfellner, E. Wilkinson, D. Correia, M. Dávila Felipe *et al.*, 2018 Renewing Felsenstein's phylogenetic bootstrap in the era of big data. Nature 556**:** 452-456.

Li, B., and C. N. Dewey, 2011 RSEM: accurate transcript quantification from RNA-Seq data with or without a reference genome. BMC bioinformatics 12**:** 323-323.

Li, H., B. Handsaker, A. Wysoker, T. Fennell, J. Ruan *et al.*, 2009 The Sequence Alignment/Map format and SAMtools. Bioinformatics (Oxford, England) 25**:** 2078-2079.

Ludewig, A. H., A. B. Artyukhin, E. Z. Aprison, P. R. Rodrigues, D. C. Pulido *et al.*, 2019 An excreted small molecule promotes *C. elegans* reproductive development and aging. Nat Chem Biol 15**:** 838-845.

Lupas, A., 1996 Prediction and analysis of coiled-coil structures. Methods in enzymology 266**:** 513-525.

Madeira, F., Y. M. Park, J. Lee, N. Buso, T. Gur *et al.*, 2019 The EMBL-EBI search and sequence analysis tools APIs in 2019. Nucleic acids research 47**:** W636-W641.

McGrath, P. T., and I. Ruvinsky, 2019 A primer on pheromone signaling in *Caenorhabditis elegans* for systems biologists. Curr Opin Syst Biol 13**:** 23-30.

McGrath, P. T., Y. Xu, M. Ailion, J. L. Garrison, R. A. Butcher *et al.*, 2011 Parallel evolution of domesticated *Caenorhabditis* species targets pheromone receptor genes. Nature 477**:** 321-325.

777 Narayan, A., G. Laurent and P. W. Sternberg, 2011 Transfer characteristics of a thermosensory
778 synapse in *Caenorhabditis elegans*. Proceedings of the National Academy of Sciences of
779 the United States of America 108**:** 9667-9672.

780 Narayan, A., V. Venkatachalam, O. Durak, D. K. Reilly, N. Bose *et al.*, 2016 Contrasting responses
781 within a single neuron class enable sex-specific attraction in *Caenorhabditis elegans*. Proc
782 Natl Acad Sci U S A 113**:** E1392-1401.

783 Nguyen, L.-T., H. A. Schmidt, A. von Haeseler and B. Q. Minh, 2015 IQ-TREE: a fast and
784 effective stochastic algorithm for estimating maximum-likelihood phylogenies. Molecular
785 biology and evolution 32**:** 268-274.

786 Noble, L. M., J. Yuen, L. Stevens, N. Moya, R. Persaud *et al.*, 2021 Selfing is the safest sex for
787 Caenorhabditis tropicalis. Elife 10.

788 Park, D., I. O'Doherty, R. K. Somvanshi, A. Bethke, F. C. Schroeder *et al.*, 2012 Interaction of
789 structure-specific and promiscuous G-protein-coupled receptors mediates small-molecule
790 signaling in *Caenorhabditis elegans*. PNAS 109**:** 9917-9922.

791 Peden, E. M., and M. M. Barr, 2005 The KLP-6 kinesin is required for male mating behaviors and
792 polycystin localization in *Caenorhabditis elegans*. Curr Biol 15.

793 Poole, R. J., E. Bashllari, L. Cochella, E. B. Flowers and O. Hobert, 2011 A Genome-Wide RNAi
794 Screen for Factors Involved in Neuronal Specification in *Caenorhabditis elegans*. PLoS
795 Genet 7**:** e1002109.

796 Powell, S., D. Szklarczyk, K. Trachana, A. Roth, M. Kuhn *et al.*, 2012 eggNOG v3.0: orthologous
797 groups covering 1133 organisms at 41 different taxonomic ranges. Nucleic acids research
798 40**:** D284-D289.

799 Pungaliya, C., J. Srinivasan, B. W. Fox, R. U. Malik, A. H. Ludewig *et al.*, 2009 A shortcut to
800 identifying small molecule signals that regulate behavior and development in
801 *Caenorhabditis elegans*. Proceedings of the National Academy of Sciences of the United
802 States of America 106**:** 7708-7713.
803 Ragsdale, E. J., M. R. Muller, C. Rodelsperger and R. J. Sommer, 2013 A developmental switch
804 coupled to the evolution of plasticity acts through a sulfatase. Cell 155**:** 922-933.
805 Reilly, D. K., D. E. Lawler, D. R. Albrecht and J. Srinivasan, 2017 Using an Adapted Microfluidic
806 Olfactory Chip for the Imaging of Neuronal Activity in Response to Pheromones in Male
807 *C. Elegans* Head Neurons. Journal of Visualized Experiments**:** e56026.
808 Reilly, D. K., E. J. McGlame, E. Vandewyer, A. N. Robidoux, C. S. Muirhead *et al.*, 2021 Distinct
809 neuropeptide-receptor modules regulate a sex-specific behavioral response to a
810 pheromone. Communications Biology 4**:** 1018.
811 Reilly, D. K., L. J. Randle and J. Srinivasan, 2019 Evolution of hermaphroditism decreases
812 efficacy of Ascaroside#8-mediated mate attraction in *Caenorhabditis* nematodes.
813 microPublication Biology.
814 Robertson, H. M., and J. H. Thomas, 2006 The putative chemoreceptor families of *C. elegans*.
815 WormBook**:** 1-12.
816 Rual, J. F., J. Ceron, J. Koreth, T. Hao, A. S. Nicot *et al.*, 2004 Toward improving *Caenorhabditis*
817 *elegans* phenome mapping with an ORFeome-based RNAi library. Genome Res 14**:** 2162-
818 2168.
819 Sammut, M., S. J. Cook, K. C. Q. Nguyen, T. Felton, D. H. Hall *et al.*, 2015 Glia-derived neurons
820 are required for sex-specific learning in C. elegans. Nature 526**:** 385-390.

Schmitz, C., P. Kinge and H. Hutter, 2007 Axon guidance genes identified in a large-scale RNAi screen using the RNAi-hypersensitive *Caenorhabditis elegans* strain *nre-1(hd20) lin-15b(hd126)*. Proceedings of the National Academy of Sciences 104**:** 834-839.

Schroeder, N. E., R. J. Androwski, A. Rashid, H. Lee, J. Lee *et al.*, 2013 Dauer-specific dendrite arborization in C. elegans is regulated by KPC-1/Furin. Curr Biol 23**:** 1527-1535.

Schwarz, E. M., M. Kato and P. W. Sternberg, 2012 Functional transcriptomics of a migrating cell in Caenorhabditis elegans. Proceedings of the National Academy of Sciences of the United States of America 109**:** 16246-16251.

Taylor, S. R., G. Santpere, A. Weinreb, A. Barrett, M. B. Reilly *et al.*, 2021 Molecular topography of an entire nervous system. Cell 184**:** 4329-4347.e4323.

Tenor, J. L., and A. Aballay, 2008 A conserved Toll-like receptor is required for Caenorhabditis elegans innate immunity. EMBO Rep 9**:** 103-109.

von Reuss, S. H., N. Bose, J. Srinivasan, J. J. Yim, J. C. Judkins *et al.*, 2012 Comparative Metabolomics Reveals Biogenesis of Ascarosides, a Modular Library of Small-Molecule Signals in *C. elegans*. Journal of the American Chemical Society 134**:** 1817-1824.

von Reuss, S. H., and F. C. Schroeder, 2015 Combinatorial chemistry in nematodes: modular assembly of primary metabolism-derived building blocks. Natural product reports 32**:** 994-1006.

Wang, J., R. Kaletsky, M. Silva, A. Williams, L. A. Haas *et al.*, 2015 Cell-Specific Transcriptional Profiling of Ciliated Sensory Neurons Reveals Regulators of Behavior and Extracellular Vesicle Biogenesis. Curr Biol 25**:** 3232-3238.

Wang, J., M. Silva, L. A. Haas, N. S. Morsci, K. C. Q. Nguyen *et al.*, 2014 *C. elegans* Ciliated Sensory Neurons Release Extracellular Vesicles that Function in Animal Communication. Current Biology 24**:** 518-525.

Wang, X., J. F. Greenberg and H. M. Chamberlin, 2004 Evolution of regulatory elements producing a conserved gene expression pattern in *Caenorhabditis*. Evolution & Development 6**:** 237-245.

White, J. G., E. Southgate, J. N. Thomas and S. Brenner, 1986 The structure of the nervous system of the nematode Caernorhabditis elegans. Phil Trans Royal Soc Lon 314B.

Wootton, J. C., 1994 Non-globular domains in protein sequences: automated segmentation using complexity measures. Computers & chemistry 18**:** 269-285.

Zhang, Y. K., D. K. Reilly, J. Yu, J. Srinivasan and F. C. Schroeder, 2019 Photoaffinity probes for nematode pheromone receptor identification. Journal of Organic & Biomolecular Chemistry**:** 10.1039/C1039OB02099C.

Zhang, Y. K., M. A. Sanchez-Ayala, P. W. Sternberg, J. Srinivasan and F. C. Schroeder, 2017 Improved Synthesis for Modular Ascarosides Uncovers Biological Activity. Org Lett 19**:** 2837-2840.

Zwaal, R. R., J. E. Mendel, P. W. Sternberg and R. H. Plasterk, 1997 Two neuronal G proteins are involved in chemosensation of the *Caenorhabditis* elegans Dauer-inducing pheromone. Genetics 145**:** 715-727.

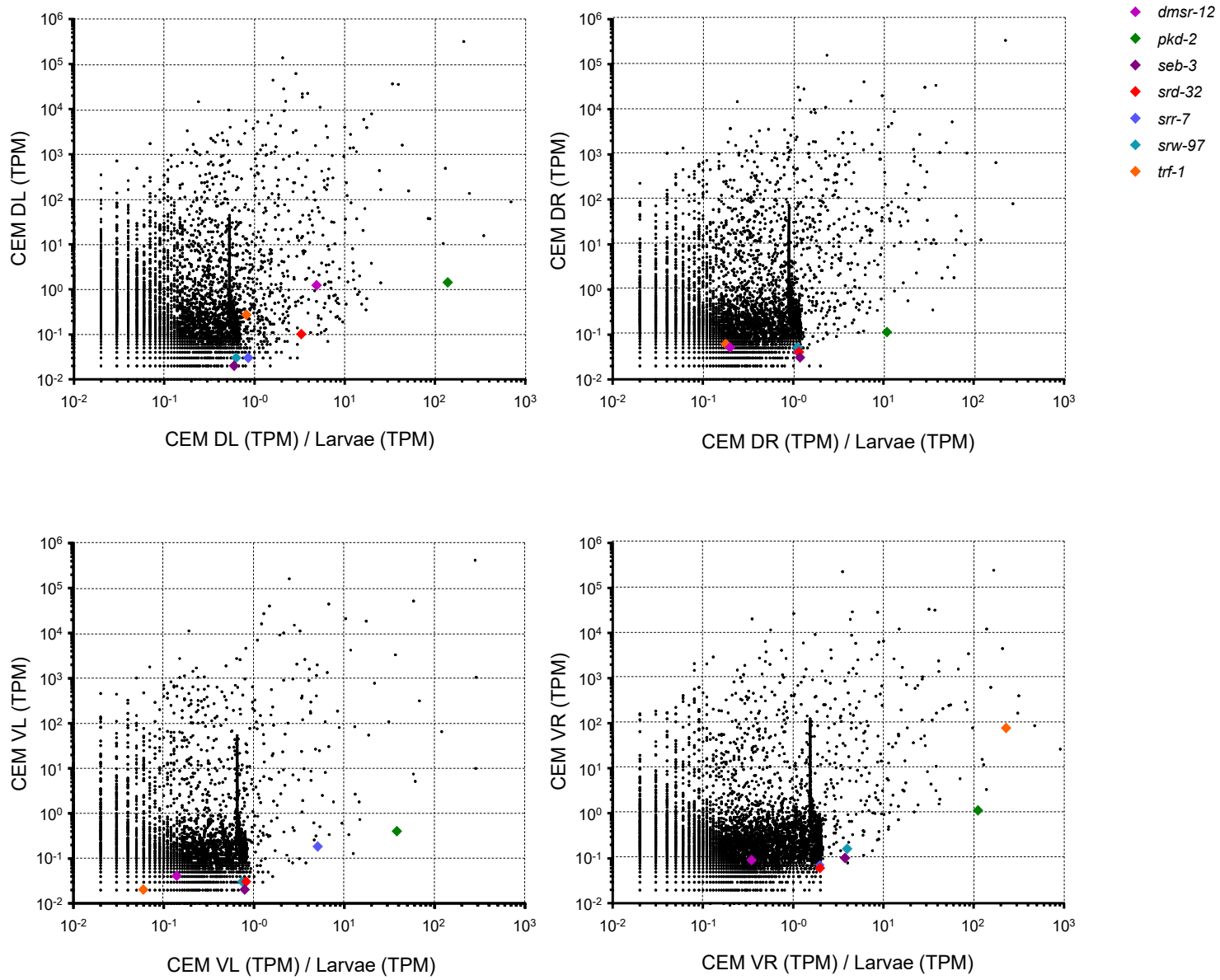
CEM DL (TPM)
CEM DL (TPM) / Larvae (TPM)
CEM DR (TPM)
CEM DR (TPM) / Larvae (TPM)
CEM VL (TPM)
CEM VL (TPM) / Larvae (TPM)
CEM VR (TPM)
CEM VR (TPM) / Larvae (TPM)
dmsr-12
pkd-2
seb-3
srd-32
srr-7
srw-97
trf-1

Figure - 1

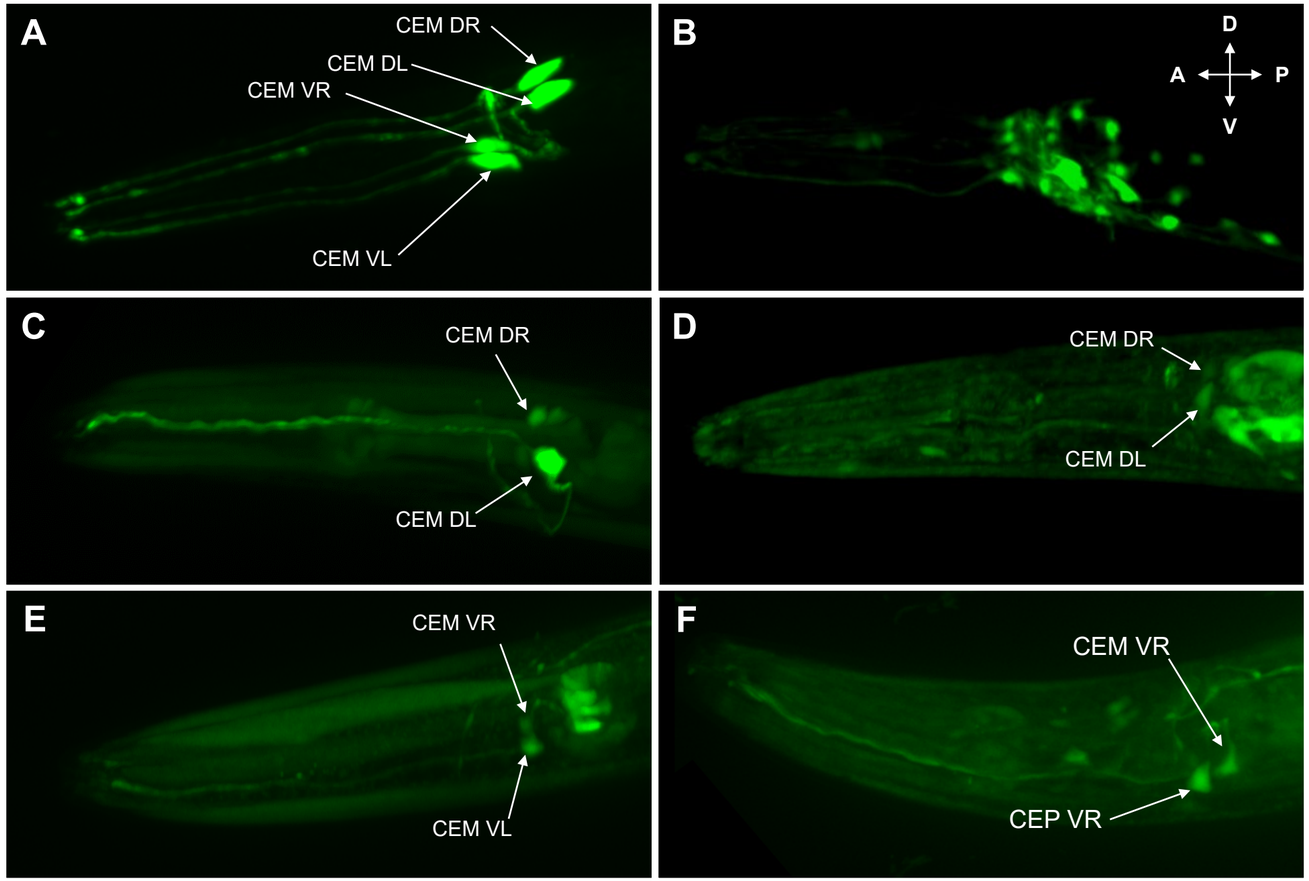

Figure - 2

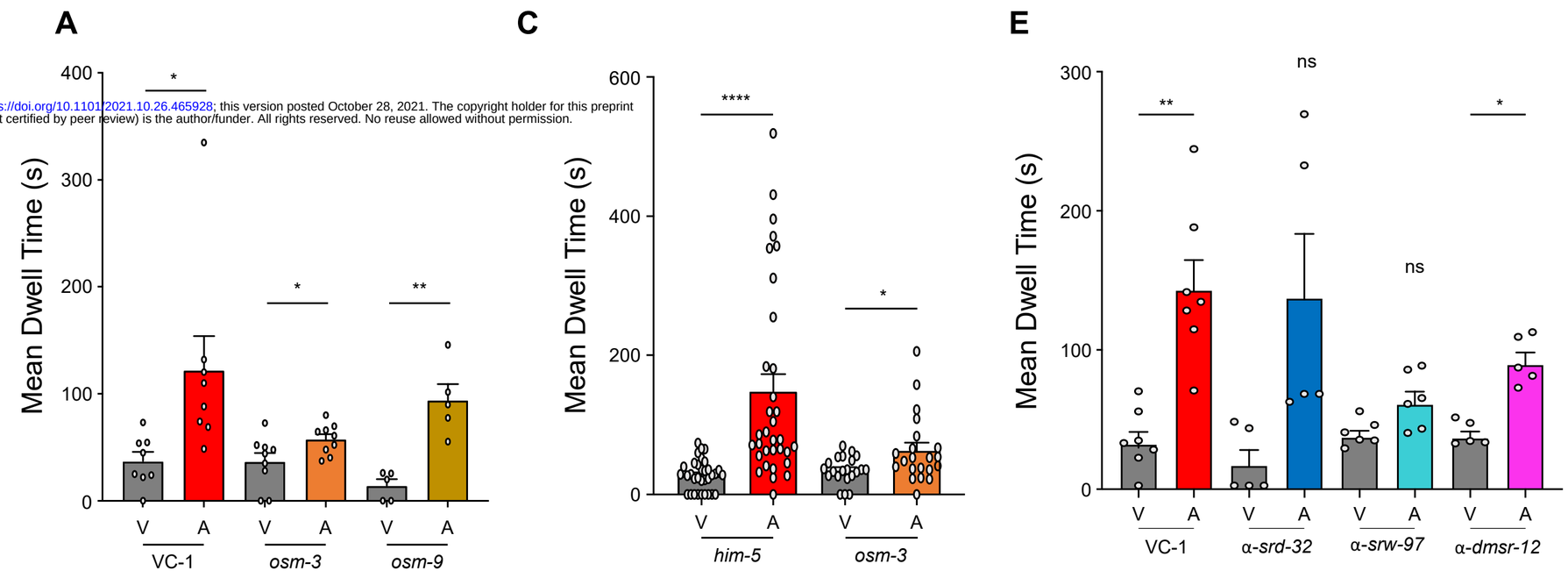

Figure - 3

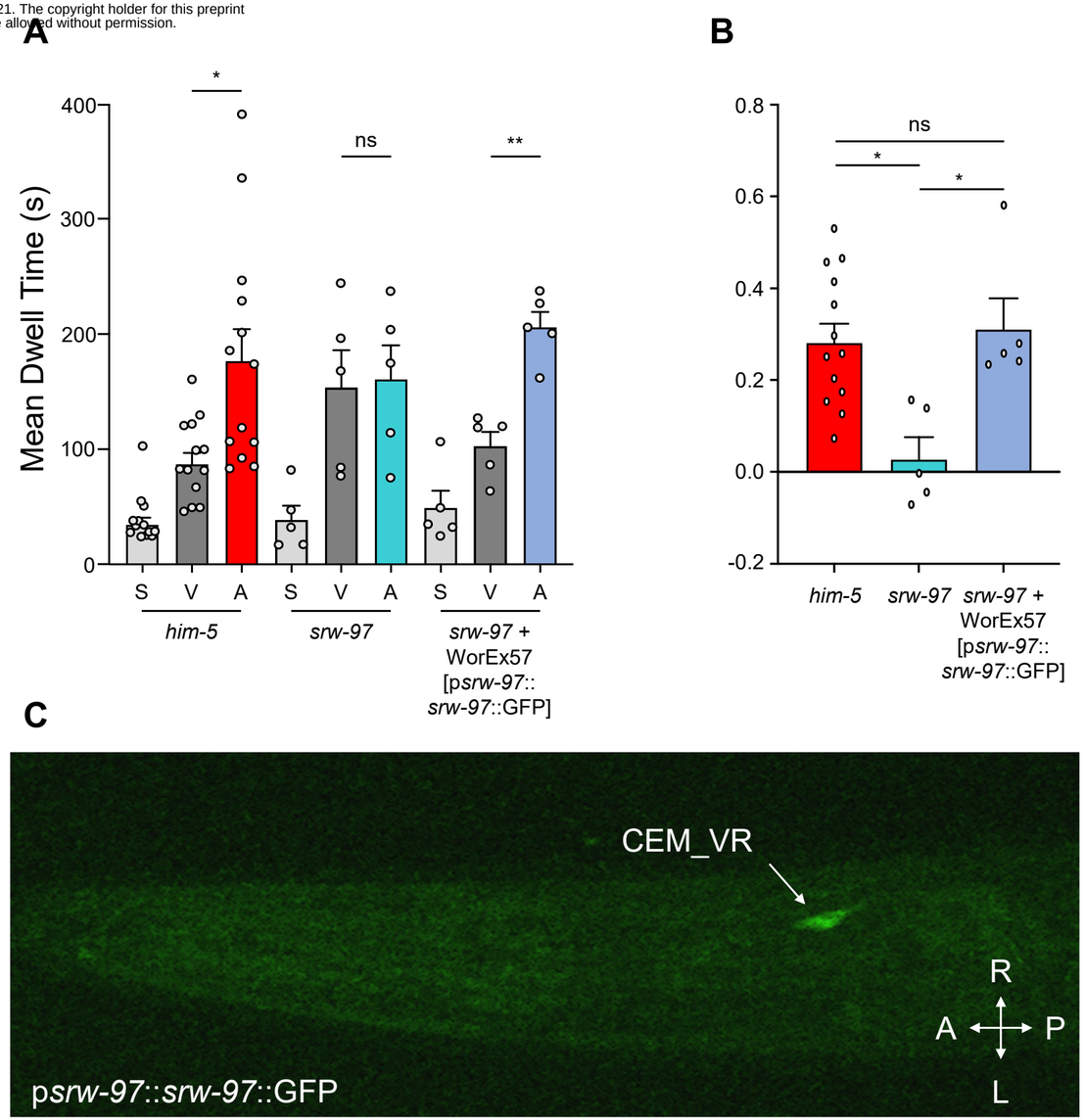

Figure - 4

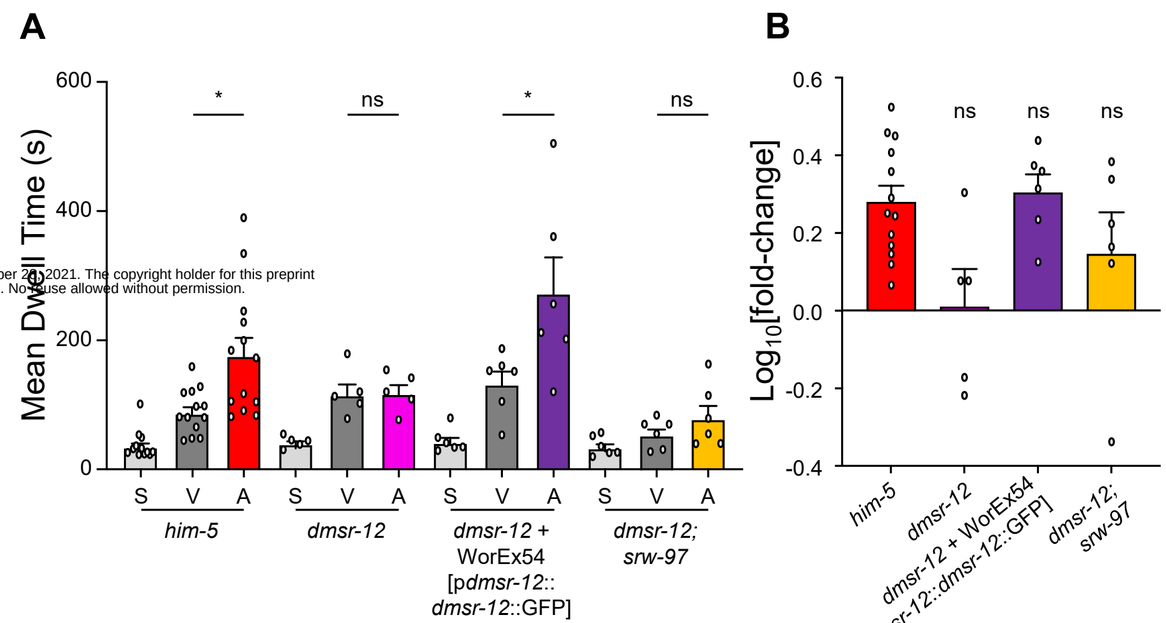

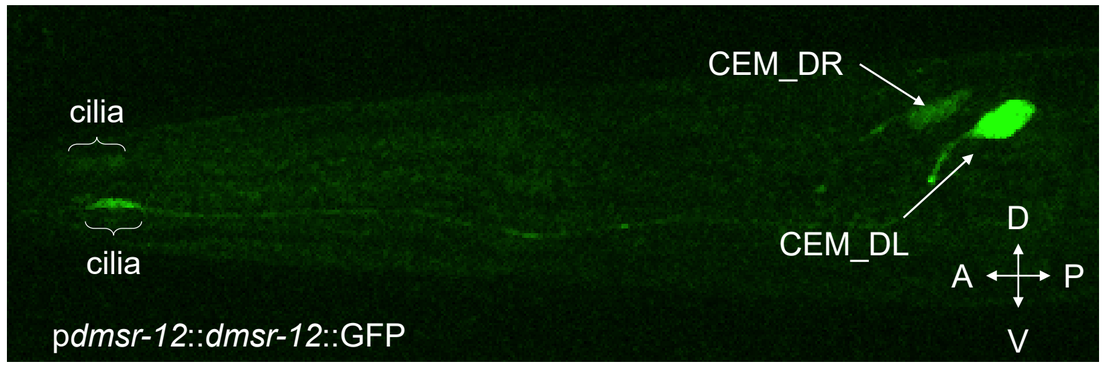

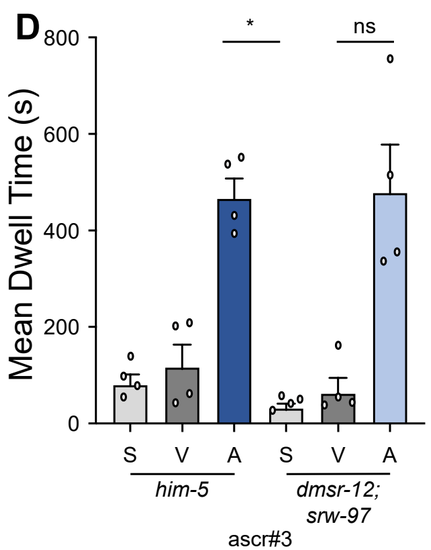

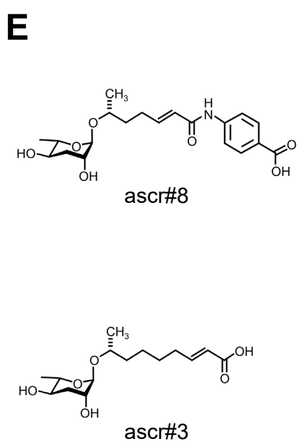

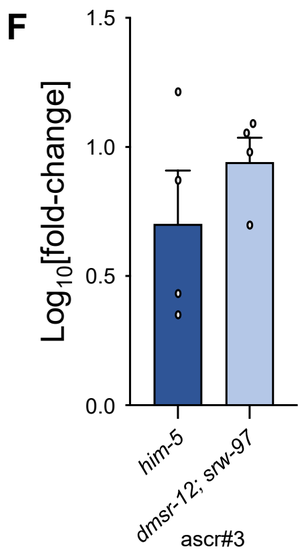

Figure - 5

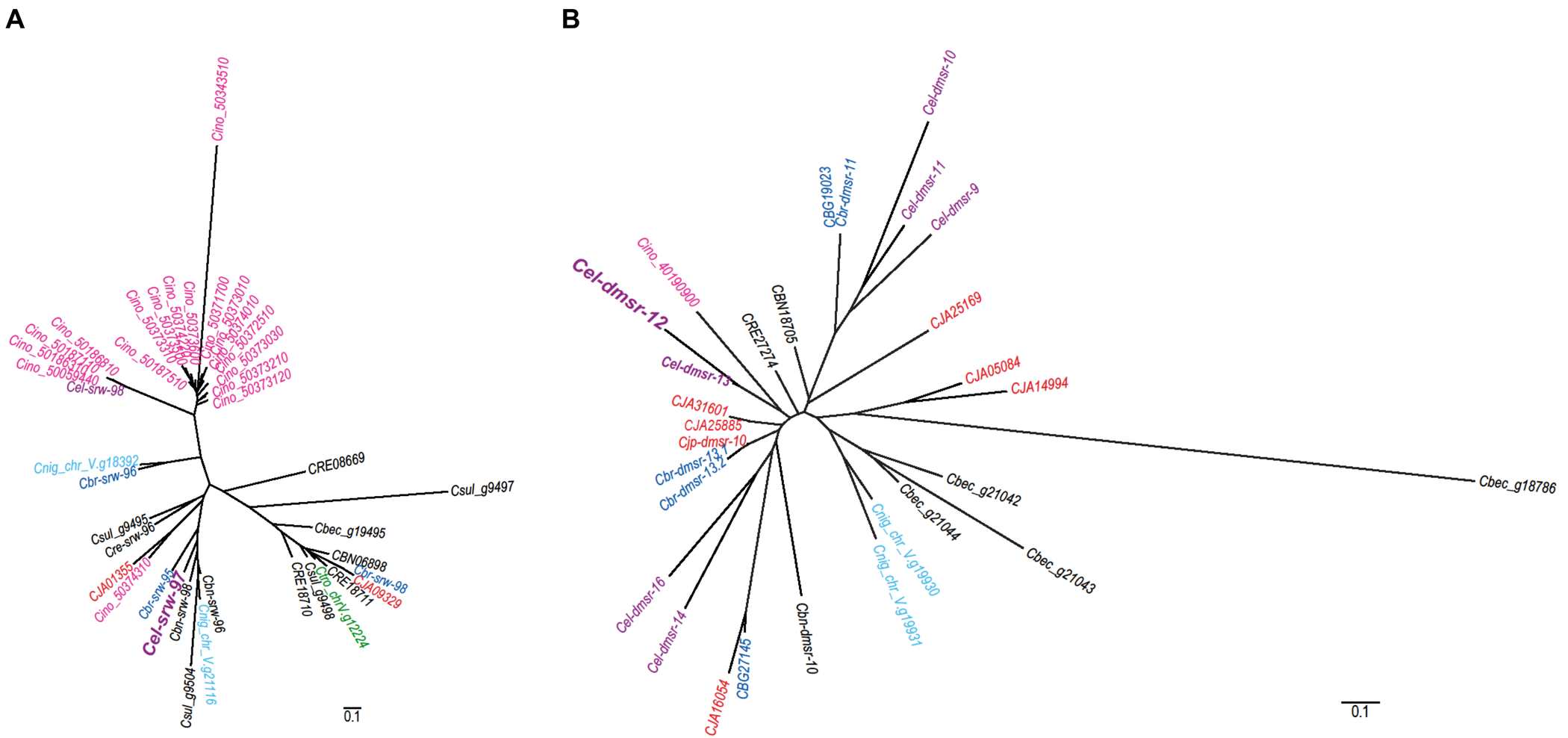

Figure - 6